Molecular Basis of Zinc-Dependent Endocytosis of Human ZIP4 Transceptor

Chi Zhang[1], **Dexin Sui**[1], **Tuo Zhang**[1], **Jian Hu**[1,2,3,*]

[1]Department of Biochemistry and Molecular Biology, Michigan State University, East Lansing, MI 48824, USA

[2]Department of Chemistry, Michigan State University, East Lansing, MI 48824, USA

[3]Lead Contact

SUMMARY

Nutrient transporters can be rapidly removed from the cell surface via substrate-stimulated endocytosis as a way to control nutrient influx, but the molecular underpinnings are not well understood. In this work, we focus on zinc-dependent endocytosis of human ZIP4 (hZIP4), a zinc transporter that is essential for dietary zinc uptake. Structure-guided mutagenesis and internalization assay reveal that hZIP4 per se acts as the exclusive zinc sensor, with the transport site's being responsible for zinc sensing. In an effort of seeking sorting signal, a scan of the longest cytosolic loop (L2) leads to identification of a conserved Leu-Gln-Leu motif that is essential for endocytosis. Partial proteolysis of purified hZIP4 demonstrates a structural coupling between the transport site and the L2 upon zinc binding, which supports a working model of how zinc ions at physiological concentration trigger a conformation-dependent endocytosis of the zinc transporter. This work provides a paradigm on post-translational regulation of nutrient transporters.

In Brief

Cell surface expression of ZIP4, a transporter for intestinal zinc uptake, is regulated by zinc availability. Zhang et al. report that human ZIP4 acts as the exclusive zinc sensor in initiating the zinc-dependent endocytosis, and a cytosolic motif is essential for sorting signal formation, indicating that ZIP4 is a transceptor.

Graphical Abstract
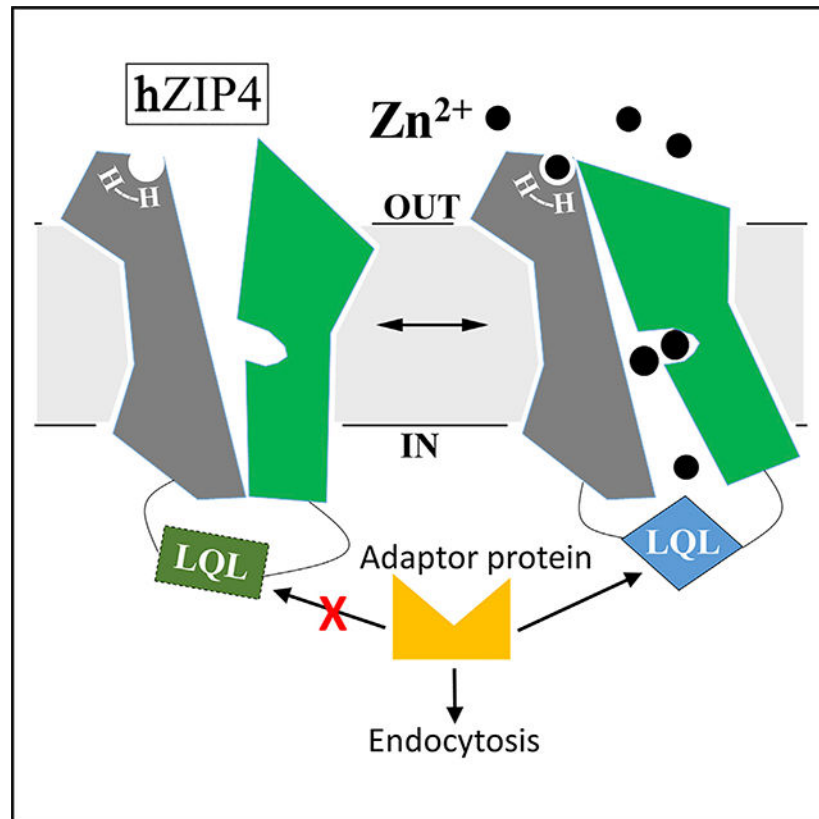
INTRODUCTION

Zinc is a micronutrient that is vital for life. The unique properties of zinc ions have been exploited for catalysis, macromolecules structure stabilization, and cell signaling. To maintain systemic and cellular zinc homeostasis and allow signaling functions of zinc ions, zinc transporters play central roles by controlling zinc flux through membranes (Bafaro et al., 2017; Hara et al., 2017; Kambe et al., 2004, 2014, 2015; Lichten and Cousins, 2009; Liuzzi and Cousins, 2004). In humans, the 14 members in the Zrt-/Irt-like protein (ZIP) family govern zinc influx from extracellular milieu or intracellular organelles/vesicles (Eide et al., 1996; Grotz et al., 1998; Jeong and Eide, 2013; Takagishi et al., 2017). As for many other nutrient transporters, the ZIPs are transcriptionally and post-translationally regulated by the availability of zinc (and other substrates, such as iron) (Chowanadisai et al., 2013; Connolly et al., 2002; Gaither and Eide, 2001; Hashimoto et al., 2015, 2016; Huang and Kirschke, 2007; Liu et al., 2008; Milon et al., 2001; Pocanschi et al., 2013; Wang et al., 2004a; Weaver and Andrews, 2012; Zhao et al., 2014). For instance, the mRNA level of ZIP4, which is exclusively responsible for zinc uptake from food, is increased drastically under zinc restriction condition because of an improved mRNA stability (Weaver et al., 2007). An alternative mechanism involves a zinc-finger transcription factor, the Krüppel-like factor 4, which was reported to be responsible for the increased ZIP4 transcription in mouse intestine at zinc deficiency (Liuzzi et al., 2009). Post-translational regulation of ZIP4 was initially reported in an *in vivo* study (Dufner-Beattie et al., 2003), followed by cultured

cellbased research, which established that zinc repletion induces ZIP4 removal from the cell surface through endocytosis, whereas zinc depletion increases ZIP4 surface level by recycling the internalized ZIP4 back to cell surface (Andrews, 2008; Kim et al., 2004; Mao et al., 2007; Weaver et al., 2007). Compared with the relative slow transcriptional regulation, the post-translational regulation represents a mechanism of rapid adjustment of zinc uptake capability taking place within minutes, therefore allowing adequate zinc uptake while protecting cells from excessive zinc-induced toxicity. Misregulation of human ZIP4 (hZIP4) endocytosis caused by dysfunctional mutations has been linked to a life-threatening recessive genetic disorder, acrodermatitis enteropathica (AE) (Dufner-Beattie et al., 2003, 2007; Geiser et al., 2012; Küry et al., 2002; Wang et al., 2002, 2004b). Interestingly, the previous study has suggested that the cell surface level of hZIP4 is regulated by two distinct post-translational mechanisms, depending on zinc level. Zinc exposure at low concentration (low micromolar) initiates hZIP4 endocytosis but without degradation, whereas exposure at high zinc concentration (tens of micromolar or higher) results in endocytosis followed by degradation (Mao et al., 2007). To distinguish these two processes, we refer to the former as zinc-dependent endocytosis and the latter as zinc-induced degradation. Similar to the substrate-stimulated endocytosis and degradation of many nutrient transporters, including the ZIPs from *Arabidopsis* (Dubeaux et al., 2018) and yeast (Gitan and Eide, 2000), zinc-induced degradation of hZIP4 depends on ubiquitination and an elevated cytosolic substrate (zinc) concentration (Mao et al., 2007). Nevertheless, zinc-dependent endocytosis of hZIP4 is still poorly understood, although it likely represents a critical regulation mechanism under physiological conditions.

In this work, we aim to address the following two important questions associated with zinc-dependent endocytosis of hZIP4: What is the molecular mechanism of zinc sensing? And which part of the cargo (hZIP4) is recognized by the endocytic machinery? Guided by an hZIP4 structural model based on our recent studies (Zhang et al., 2016, 2017), we carried out extensive mutagenesis, internalization assay, and biochemical studies on hZIP4 expressed in a human cell line. Our data revealed that: (1) hZIP4 acts as the only zinc sensor during zinc-dependent endocytosis, indicating that hZIP4 can be categorized as a transceptor exerting both transport and sensing functions; (2) a conserved Leu-Gln-Leu (LQL) motif in the second cytosolic loop (L2) is required for hZIP4 constitutive endocytosis; and (3) the transport site in the transmembrane domain (TMD) is structurally coupled with the L2. Based on these findings, we propose that the conformational change of hZIP4 induced by zinc binding at the transport site allows an LQL motif-mediated ubiquitination-independent endocytosis, representing an additional mechanism of post-translational regulation of a nutrient transporter.

RESULTS

Constitutive hZIP4 Endocytosis Is Largely Diminished upon Intracellular/Extracellular Zinc Depletion

We stably expressed hZIP4 with a C-terminal hemagglutinin (HA) tag in HEK293 cells and examined endocytosis by monitoring anti-HA antibody internalization as reported previously (Wang et al., 2004a). Under the basal condition (regular DMEM-fetal bovine serum [FBS]

cell culture medium), we found that hZIP4-HA underwent a constitutive endocytosis (Figure 1A), which can likely be attributed to the low micromolar zinc concentration in this culture medium (Richardson et al., 2018). Adding 1 or 10 μM zinc to the cells did not affect endocytosis or hZIP4 cell surface level. We did not add more zinc because it may stimulate zinc-induced degradation (Mao et al., 2007). Similarly, after incubation with the Chelex-treated culture medium (metal-free medium) for 15 min, adding zinc in the medium did not affect endocytosis or surface level, which indicates that zinc removal from the extracellular environment has no immediate effects on hZIP4 trafficking. In sharp contrast, after the treatment with 20 μM N,N,N',N'-tetrakis(2-pyridylmethyl)ethane-1,2-diamine (TPEN), which is a cell membrane-permeable high-affinity zinc chelator, in the regular culture medium for 15 min, as low as 1 μM zinc can restore hZIP4 endocytosis, and the cell surface level of hZIP4 was concomitantly reduced. Further experiments showed that TPEN treatment drastically reduced hZIP4 endocytosis, and 10 μM zinc restored it to the level under the basal condition, with the hZIP4 surface level being restored as well (Figure 1B). Consistent with the western blot results, immunofluorescence analysis showed that the amount of internalized anti-HA antibody decreased significantly after TPEN treatment, whereas zinc supplement reversed the effects of zinc depletion (Figure 1C). In order to exclude the possibility that acute zinc depletion by TPEN has a general inhibitory effect on endocytosis, we tested internalization of the Alexa 488-labeled transferrin under the same experimental conditions and did not observe a defect in transferrin internalization, which is consistent with a previous report that TPEN treatment did not affect trafficking of several other irrelevant membrane proteins (Kim et al., 2004). Collectively, these data suggest that there must be a specific zinc-sensing mechanism through which hZIP4 endocytosis is largely diminished by zinc depletion in both intracellular and extracellular pools. To estimate zinc binding affinity of the putative zinc sensor, we conducted dose-dependent experiments. By plotting the internalized anti-HA antibody against the extracellular zinc concentrations, we obtained an apparent zinc dissociation constant (K_D) of 1.5 μM by curve fitting using the Michaelis-Menten model (Figure S1A). It should be noted that, given that the Chelex-treated culture medium contains many potential zinc binding proteins (such as bovine serum albumin from FBS, which binds zinc with a low micromolar affinity; Goumakos et al., 1991; Lu et al., 2008), the putative zinc sensor must be of high affinity toward zinc ions.

hZIP4 Is the Exclusive Zinc Sensor in Zinc-Dependent Endocytosis

Theoretically, many proteins involved in endocytosis may sense zinc if high-affinity zinc binding alters their functional states. Inspired by the fact that some disease-causing mutations of hZIP4 impair zinc sensing in zinc-dependent endocytosis (Wang et al., 2004b), we wondered whether hZIP4 plays a direct role in zinc sensing. To test this hypothesis, we conducted structure-guided mutagenesis on hZIP4 by using a structure model built on the prior structural studies of the ZIP proteins (Figure 2A). The structural models of the N-terminal extracellular domain (ECD) and the C-terminal TMD are derived from the crystal structures of a bat ZIP4-ECD (Zhang et al., 2016) and a prokaryotic ZIP (Zhang et al., 2017), respectively, via homology modeling. We also adopted a proposed dimerization model of hZIP4 (Antala et al., 2015). This coevolution-based computational model has shown an impressive similarity to the overall fold of the prokaryotic ZIP determined crystallographically (Zhang et al., 2017). Based on this model, we identified four

hypothetical high-affinity zinc binding sites, including a histidine-rich loop in the ECD (region I), a putative extracellular metal binding site between TM2 and TM3 (region II), the transport site in the middle of the transport pathway (region III), and a histidine-rich segment in a cytosolic loop between TM3 and TM4 (region IV) (Figure 2A).

We then conducted mutagenesis to examine which region(s) is responsible for zinc sensing in zinc-dependent endocytosis. For quantitative analysis, we defined zinc-sensing capability as a ratio of the difference between endocytosis with and without zinc over the endocytosis level when zinc is present (see equation in STAR Methods). For the wild-type hZIP4, this ratio generally falls within the range of 0.5–0.8, which is consistent with the estimation that hZIP4 endocytosis rate was reduced by three to four times upon zinc depletion (Figure S3). Most of the mammalian ZIP4 proteins have a histidine-rich loop in their ECDs (region I) (Antala and Dempski, 2012; Kambe and Andrews, 2009; Zhang et al., 2016), and the structural model of hZIP4 suggests that this highly flexible loop is likely right on the top of the entrance of the transport pathway, and our recent study has shown that it binds zinc ions with low micromolar affinity and plays a role in zinc transport (Zhang et al., 2019). We generated a mutant with all four histidine residues (H238, H241, H243, and H245) replaced with serine residues. In the internalization assay conducted on the cells stably expressing this mutant, we did not see any defect in zinc sensing (Figure 2B). As a matter of fact, deletion of the whole ECD (ECD) had little effect on zinc sensing (Figure 2C), excluding the possibility that ZIP4-ECD acts as a zinc sensor in zinc-dependent endocytosis. We also noticed that ECD has a higher endocytosis level under the basal condition than the wild-type hZIP4, which may be attributed to the higher expression level of ECD (Zhang et al., 2016). A report on mouse ZIP4 also showed an increased endocytosis upon ECD deletion (Chun et al., 2019), and the authors proposed that the ECD may play a negative role in ZIP4 endocytosis. In addition, iron sensing in iron-stimulated hZIP14 endocytosis relies on N-glycosylation of N102 in the ECD (Zhao et al., 2014). Therefore, it seems that the ECD of the ZIPs may have different roles in ZIP trafficking.

Region II is a short extracellular loop harboring two highly conserved histidine residues in an HxH motif (H388 and H390). The previous mutagenesis study on IRT1 from *Arabidopsis thaliana* has suggested that this loop is involved in substrate recognition (Rogers et al., 2000). The study on mouse ZIP4 showed that mutating the HxH motif significantly reduced but did not eliminate zinc sensing (Chun et al., 2019). In this work, we found that substituting both histidine residues with alanine residues (H388A/H390A) did not affect zinc sensing (Figures 2D and S1C). It seems that the HxH motif differentially contributes to zinc sensing among ZIP4 homologs. In mouse ZIP4, although the HxH motif is not absolutely required for zinc sensing, it does play a role in zinc-dependent endocytosis; whereas in hZIP4, the contribution of the HxH motif to zinc sensing is too little to be detected. Such a discrepancy may be attributed to the difference in amino acid sequence between the two close homologs. Notably, the loop connecting TM2 and TM3 (where the HxH motif resides) in hZIP4 is eight residues shorter than the counterpart in mouse ZIP4 (Figure S2). Indeed, the two proteins are less similar in this region than in other regions, which may account for the distinct functions.

The second conserved histidine-rich segment (region IV) is on the second cytosolic loop connecting TM3 and TM4 (referred to as L2), which is a characteristic feature of many ZIP family members (Jeong and Eide, 2013). It has been shown that the metal chelating residues in the L2 bind zinc with nanomolar affinity (Bafaro et al., 2015, 2019) and are required for zinc-induced hZIP4 degradation (Mao et al., 2007). However, diminishing zinc binding capability of the L2 by replacing all five histidine residues (H438, H441, H443, H446, and H448) with glycine residues did not affect either endocytosis or zinc sensing (Figure 2E), which is consistent with the result of alanine substitution of these histidine residues in hZIP4 (Mao et al., 2007). Because C436 has been indicated to solely confer nanomolar affinity toward zinc ion for the isolated L2 peptide (Bafaro et al., 2015, 2019), we generated the C436A variant and the C436A/H438G/H441G/H443G/H446G/ H448G variant for which zinc binding at the L2 is supposed to be greatly abrogated and completely eliminated, respectively. As shown in Figures 2F and 2G, no defect in zinc sensing can be detected for these two variants. Therefore, it is unlikely that the metal chelating residues in the L2 are directly involved in zinc sensing in zinc-dependent endocytosis.

In the crystal structure of a prokaryotic ZIP from *Bordetella bronchiseptica*, we identified a binuclear metal center (BMC) within the transport pathway (Zhang et al., 2017). Because the residues contributive to the BMC are also conserved in hZIP4 and many other ZIPs, we were able to generate a BMC structural model of hZIP4 (region III) and demonstrated its importance in zinc transport (Zhang et al., 2017). Particularly, D511 appears to be a key residue bridging the two metal binding sites, and the D511A variant loses most of the zinc transport activity, probably because of disruption of both metal binding sites. We therefore focused on the D511A variant to test the role of the BMC in zinc sensing. In sharp contrast with the wild-type protein, the D511A mutant can be efficiently endocytosed not only at the basal condition or in the zinc-supplemented Chelex-treated medium, but also in the absence of zinc (Figure 2H). Adding zinc up to 60 μM did not change the endocytosis level, confirming a loss of zinc-sensing function. Therefore, endocytosis of the D511A mutant becomes a zinc-independent process. This result strongly suggests that, among many players in zinc-dependent endocytosis, hZIP4 per se is the only zinc sensor in this process because the D511A mutation on hZIP4 is enough to turn on hZIP4 endocytosis even in the absence of zinc. In addition, the fact that the loss-of-function mutation (D511A) at the BMC completely abrogates zinc sensing suggests that the BMC plays a key role in zinc sensing. In our previous study, we also identified a gain-of-function H540A variant at the BMC with an increased transport rate (Zhang et al., 2017). We then tested the effects of this mutation on hZIP4 endocytosis and zinc sensing. It turned out that the H540A variant functioned as the wild-type protein with no defect in endocytosis or zinc sensing (Figures 2I and S1B). Therefore, out of the four potential high-affinity zinc binding sites, only the BMC is related with zinc sensing, and the functionality of the BMC appears to be linked with zinc-sensing capability.

Identification of the LQL Motif Essential for hZIP4 Endocytosis

It has been shown that, at the basal condition, the cell surface level of hZIP4 increased significantly when a dominant-negative dynamin K44A was overexpressed in the hZIP4-expressing cells (Mao et al., 2007). Our data showed that, as low as 6 μM (2 μg/mL)

chlorpromazine (CPZ), which specifically disrupts the clathrin-dependent endocytosis (Vercauteren et al., 2010), strongly inhibited hZIP4 internalization at the basal condition (Figure S4). These data therefore support that hZIP4 is likely endocytosed through a clathrin-dependent process where a sorting signal in the cargo protein is recognized by the adaptor proteins required for later engagement of the endocytic machinery (Traub and Bonifacino, 2013).

One well-established mechanism in cargo recognition is through a sorting motif, which is a short segment in the cytoplasmic portion of the target membrane protein. The known linear sorting motifs include YxxΦ (Φ means hydrophobic residue, and x means any residue), [D/E]xxxL[L/I] (dileucine motif), and [F/Y]xNPx[Y/F]. In the structural model of hZIP4 (Figure 2A), we found no YxxΦ or [F/Y]xNPx[Y/F] motif, but one dileucine motif (^{477}ESPELL^{482}) in the L2. A similar dileucine motif in the corresponding L2 of hZIP1 was reported to mediate endocytosis (Huang and Kirschke, 2007). However, substitution of the two leucine residues (L481 and L482) by alanine residues had no effect on hZIP4 endocytosis (Figure 3A). Ubiquitination-mediated endocytosis is another well-characterized mechanism for membrane protein internalization. It has been shown that zinc-induced degradation of yeast Zrt1 and hZIP4 are mediated by ubiquitination (Gitan and Eide, 2000; Mao et al., 2007). We then replaced the only two cytoplasmic lysine residues (K463 in the L2 and K611 in the short loop connecting TM7 and TM8; see Figure 2A) with arginine residues. However, neither the single substitutions (K463R and K611R) nor the double mutation (K463R/K611R) affected hZIP4 endocytosis (Figure 3B). Because K463 has been proposed to be ubiquitinated in zinc-induced hZIP4 degradation (Weaver et al., 2007), our result reinforces the notion that zinc-induced degradation and zinc-dependent endocytosis are fundamentally distinct processes (Liuzzi et al., 2009).

After these trials, we hypothesized that hZIP4 may possess an uncharacterized sorting motif in its cytoplasmic portion. Because the L2 is the longest cytosolic loop, we examined its importance in hZIP4 endocytosis by replacing it with a soluble and unstructured linker (GS)$_5$. The length of the GS linker was designed based on the distance between TM3 and TM4 in the structural model of hZIP4. The resulting variant (ΔL2) can be normally expressed on the cell surface, but notably, the endocytosis at the basal condition drastically decreased to a negligible level (Figure 3C). This result indicated that the L2 is indispensable for hZIP4 endocytosis and the L2, either by itself or together with another part of the protein, must be involved in the putative sorting signal. Then we conducted a non-biased scan on the L2 to identify the key residues essential for hZIP4 endocytosis. Because the L2 is composed of 60 residues, we divided the L2 into six 10-residue segments (S1–S6) and then replaced each segment by a (GS)$_5$ linker. We transiently expressed these variants in HEK293T cells for internalization assay, and the results showed that only the third segment (S3, residues 449–458) is important because endocytosis of the ΔS3 mutant was completely diminished. Sequence alignment of mammalian ZIP4 proteins showed that S3 contains four highly conserved residues (^{452}LQL^{454} and E458) (Figure 3D). We then replaced each of these four residues by an alanine respectively and found that L452A and L454A completely abrogated endocytosis, Q453A largely reduced it, whereas E458A did only moderately. Therefore, we refer to this motif as the LQL motif. It should be noted that the mutations on the L2 did not affect protein folding or trafficking, because all of the variants (including a

LQL/AAA triple mutant) can be normally expressed at the cell surface with glycosylation comparable with the wild-type protein. Notably, the LQL/AAA mutation also completely diminished endocytosis of the D511A mutant (D511A/LQL/AAA quadruple mutant; Figure 3D), which undergoes zinc-independent endocytosis (Figure 2H), indicating that the LQL motif is involved in an essential step independent from zinc sensing eliminated by the D511A mutation.

The LQL Motif Does Not Function as a Linear Sorting Motif

Next, we adapted the CD8 chimera approach to examine whether the LQL sequence functions as a linear sorting motif. The CD8 chimera internalization assay has been applied in the studies of an array of membrane proteins (Harasaki et al., 2005; Nilsson et al., 1989; Seaman, 2007) and in screens for unknown sorting motifs (Kozik et al., 2010). CD8 is a type I membrane protein with an N-terminal ECD, a single-transmembrane helix, and a short C-terminal cytosolic tail. We inserted an HA tag immediately after the signal peptide to allow the internalization assay by using the anti-HA antibody as we did on hZIP4. We first made two constructs to test the feasibility of this approach under our experimental conditions. As shown in Figure 4, CD8 without its C-terminal cytosolic tail (CD8 C, negative control) did not undergo endocytosis, whereas CD8 C fused with an FxNPxY motif (positive controls) can be efficiently endocytosed. We then generated two chimeric constructs: the CD8 C-L2 construct where the 60-residue L2 from hZIP4 was fused at the C terminus of the CD8 C, and the CD8 C-L2-AAA construct where the LQL sequence was replaced by three alanine residues. Although the chimeric proteins were expressed and presented at the cell surface, the assay showed that neither of them was substantially endocytosed and there was no difference between them. Combined with the report that the isolated L2 is an intrinsically disordered peptide (Bafaro et al., 2015), this result indicated that the LQL motif is unlikely to function as a canonical linear sorting motif. It is known that a folded domain, rather than a linear amino acid sequence, may encode a sorting signal (Miller et al., 2011; Pryor et al., 2008; Yu et al., 2010). Given the key role of the LQL motif in hZIP4 endocytosis and the absence of a functional linear sorting motif in the L2, we postulate that the LQL motif is critically contributive to a sorting signal only when it is in the context of the full-length hZIP4, probably in a folded state.

Partial Proteolysis of hZIP4 Suggests the L2 Is Structurally Coupled with the BMC upon Zinc Binding

If the LQL motif does not work as a linear sorting motif and a certain conformation of the L2 is required for engagement of endocytic machinery, a zinc-induced conformational change of the L2 would be expected. Lack of experimentally determined structure of full-length eukaryotic ZIP and the highly dynamic properties of the L2 prevent reliable modeling of the L2 in the full-length ZIP4. To investigate the putative conformational change of the L2, we applied partial proteolysis on purified hZIP4. Full-length hZIP4 with an N-terminal FLAG tag and a C-terminal HA tag (Figure 5A) was overexpressed in a human cell line (FreeStyle 293-F) and purified to homogeneity using anti-FLAG M2 affinity gel. As shown in Figure 5B, hZIP4 can be partially cleaved by chymotrypsin under an optimized condition, generating an N-terminal 50-kDa fragment with the FLAG tag and a C-terminal 20-kDa fragment with the HA tag. Based on the molecular weights of the two fragments, it can be

deduced that the proteolysis occurred at the L2. To locate the cleavage sites, we subjected the partial proteolysis product to mass spectrometry, which identified a major component corresponding to the fragment (460–482) right within the L2 (Figure 5A; Figure S5). This result indicates that the putative dileucine motif (L481 and L482) and L459 immediately downstream of the LQL motif are the most proteolysis-susceptible region in hZIP4, and it also suggests that the leucine residues in the LQL motif (L452 and L454) are more resistant to chymotrypsin, presumably due to less access to the solvent and/or a folded structure.

With the optimized experimental condition, we studied the effects of zinc ions on L2 proteolysis. As shown in Figure 5C, zinc ions effectively reduced proteolysis of the wild-type protein with an apparent half maximal effective concentration (EC_{50}) of 2 μM (Figure S6). In contrast, zinc ions up to 100 μM had no protective effect on the purified D511A mutant, which not only agrees with the observation that the D511A mutant protein loses zinc-sensing function in the internalization assay (Figure 2H), but also excludes the possibility that zinc protection against proteolysis for the wild-type protein is attributed to zinc inhibition of chymotrypsin. Collectively, these data indicate that zinc binding to the high-affinity binding site(s) of hZIP4 indeed induces conformational changes of the L2, and such a structural rearrangement can be affected by a loss-of-function mutation at the BMC, highlighting the structural coupling between the transport site in the TMD and the cytoplasmic L2.

DISCUSSION

Many nutrient transporters undergo substrate-stimulated endocytosis upon substrate repletion, which is a protective mechanism against toxic effects caused by nutrient over-absorption. However, the underlying molecular mechanism of this post-translational regulation has not been fully understood. Particularly, substrate sensing and cargo recognition by endocytic machinery are the two central questions to be answered. In this work, we addressed these issues associated with a human zinc transporter hZIP4, which is a representative member of the ZIP family and exclusively mediates the intestinal uptake of dietary zinc, an essential but potentially toxic micronutrient.

We examined the hypothesis that hZIP4 per se is a zinc sensor required for initiation of zinc-dependent endocytosis. By screening the putative zinc binding sites in the hZIP4, we found that a hZIP4 mutant (D511A) underwent a zinc-independent endocytosis (Figure 2H). Because zinc depletion by TPEN did not slow down endocytosis of the D511A mutant, the functionality of the endocytic machinery must be zinc independent and hZIP4 must function as the only zinc sensor during its endocytosis. The latter is further supported by the recent report that mutation of the two conserved extracellular histidine residues in the HxH motif reduced zinc sensing of mouse ZIP4 (Chun et al., 2019). Notably, the HxH mutation did not completely diminish zinc sensing in mouse ZIP4, and the same mutation (H388A/H390A) in hZIP4 did not affect endocytosis elicited by 10 μM zinc (Figure 2D), indicating the HxH motif is not an essential element for zinc sensing. In contrast, a complete loss of zinc-sensing function of the D511A mutant suggests that the BMC (the transport site) likely plays a more critical role in zinc sensing. The transport site meets two major requirements for a zinc sensor functioning at low micromolar zinc concentration: high affinity toward zinc ions

and zinc-binding-induced conformational change. First, according to our structural model, the transport site of hZIP4 is composed of several metal chelating residues, suggestive of a high-affinity zinc binding site. It is notable that the apparent K_D of the zinc sensor (1.5 μM) is close to the apparent K_m of the transporter (~2 μM) (Zhang et al., 2016, 2017), supporting the transport site being used as the zinc sensing site. Second, as established for many solute carrier proteins, substrate binding at the transport site likely induces a global conformational switch, thus allowing translating zinc binding to a structural rearrangement of the L2. The partial proteolysis results not only indicated that zinc binding indeed induces hZIP4 conformational change, but also loss of zinc-sensing functions for the D511A mutant provided direct evidence supporting a structural coupling between the BMC and the L2 (Figure 5). In addition, because the transport site is accessible to both intracellular and extracellular zinc pools, zinc sensing through it also explains the necessity of zinc depletion from both intracellular and extracellular pools (by TPEN treatment) to drastically reduce hZIP4 endocytosis (Figures 1A and 1B). Taken together, hZIP4 can be viewed as a transceptor, because it is not only a functional transporter but also a receptor-making response to changed zinc availability for self-regulation.

It has been shown that the substrate-induced conformational change is required for substrate-stimulated endocytosis of many yeast nutrient transporters/transceptors (Cain and Kaiser, 2011; Ghaddar et al., 2014; Gournas et al., 2017; Guiney et al., 2016; Keener and Babst, 2013; Talaia et al., 2017). For instance, arginine binding on Can1, an arginine permease, induces a conformational change to unmask a segment in the N-terminal cytosolic region for α-arrestin Art1 binding, followed by recruitment of an E3 ligase Rsp5 for ubiquitination and endocytosis (Gournas et al., 2017). An increased intracellular concentration of arginine is also required to activate Art1 via stimulating TORC1. Thus, a "double-lock" mechanism has been proposed for Can1 and other amino acid permeases within the amino acid, polyamine, and organocation (APC) transporter family (Gournas et al., 2017). In contrast with these well-characterized nutrient transceptors exerting both transport and signaling functions, zinc-dependent hZIP4 endocytosis must follow a distinct mechanism for three reasons. First, hZIP4 endocytosis is not ubiquitination dependent. Ubiquitination occurs on one or multiple lysine residues in cargo proteins. We found that the mutations of the cytoplasmic lysine residues (K463 and K611) did not affect hZIP4 endocytosis (Figure 3B). Consistently, replacing the fourth segment (S4), which contains the only lysine residue (K463) in the L2, by a $(GS)_5$ linker did not affect endocytosis (Figure 3C). These data essentially exclude the possibility that zinc-dependent hZIP4 endocytosis is mediated by ubiquitination. Our observation is also consistent with the previous report that the K476A mutation in the L2 of mouse ZIP4 (equivalent to K463 in hZIP4) did not affect the ectodomain shedding, which is an endocytosis-dependent process (Kambe and Andrews, 2009). The ubiquitination-independent endocytosis of a nutrient transporter is unusual because substrate-stimulated endocytosis of many other nutrient transporters depends on ubiquitination (Eguez et al., 2004; Erpapazoglou et al., 2008; Felice et al., 2005; Fujita et al., 2018; Galan et al., 1996; Gitan and Eide, 2000; Graschopf et al., 2001; Liu et al., 2007; Soetens et al., 2001). As far as we know, the only exception is the human copper transporter hCTR1, which reportedly undergoes endocytosis without degradation or ubiquitination upon low micromolar copper exposure for a short period of time (Clifford et al., 2016; Molloy and Kaplan, 2009).

However, high-concentration copper exposure for a prolonged period of time induces hCTR1 degradation (Guo et al., 2004), and copper-induced degradation of the yeast CTR1 was shown to be ubiquitination dependent (Liu et al., 2007). Second, as demonstrated in the case of the D511A mutant, hZIP4 endocytosis does not rely on an increased intracellular concentration of zinc to activate a downstream signaling process, whereas the proposed "double-lock" mechanism for the yeast APC transporters requires an elevated intracellular substrate concentration to activate TORC1 and then Art1 for Rsp5 recruitment (Gournas et al., 2017). Third, hZIP4 endocytosis is mediated through a sorting signal encoded in the long cytosolic loop L2. A thorough scan of the L2 led to the identification of the LQL motif essential for hZIP4 endocytosis (Figure 3C). Importantly, because the isolated and unstructured L2 fused at the C terminus of CD8 did not induce endocytosis of the chimera (Figure 4), this conserved motif is unlikely to function as a canonical linear sorting motif. Instead, a folded LQL motif is probably required to form a functional sorting signal, either by itself or together with other regions of the full-length hZIP4.

Based on these findings, we here propose a working mechanism of zinc-dependent hZIP4 endocytosis (Figure 6). Under the basal condition, zinc binding to the transport site (and probably the extracellular HxH motif concomitantly) of hZIP4 triggers a conformational change in the TMD, which makes the LQL motif fold into a certain conformation so that hZIP4 becomes recognizable by endocytic machinery. Conversely, zinc removal from the zinc sensing site(s) may favor an alternative conformation where the LQL motif-involved sorting signal is not functional. Because zinc-dependent hZIP4 endocytosis can be triggered by low micromolar zinc in the presence of serum, it may represent an important post-translational regulation mechanism, which is impaired by some AE-causing mutations (Wang et al., 2004b). As such, dysregulation of this mechanism may contribute to AE pathology. Although the current data strongly indicate that hZIP4 functions as the exclusive zinc sensor in initiating the zinc-dependent endocytosis, we cannot exclude the possibility that cell surface expression of hZIP4 may also be regulated by yet-to-be-identified proteins that participate in other steps of membrane protein trafficking (such as recycling) in a zinc-dependent manner. Should these proteins be identified, it would be interesting to examine whether they directly or indirectly bind hZIP4 as a way to exert their regulatory functions. This work also reinforces the notion that hZIP4 is internalized through two distinct mechanisms depending on zinc levels: ubiquitination-independent constitutive endocytosis at a physiological zinc concentration and ubiquitination-dependent zinc-induced degradation at a toxic zinc concentration (Mao et al., 2007). The latter has been proposed to be achieved through a structural remodeling of K463 (K476 in mouse ZIP4) in the L2 triggered by intracellular zinc binding to the cytoplasmic histidine-rich segment. Therefore, both mechanisms are centered on the L2 (Figure 6). Sequence comparison of the 14 hZIPs showed that only hZIP12, which is the closest homolog of hZIP4, has a conserved "[509]IQL" motif in the corresponding cytosolic loop, suggesting that the other hZIPs expressed at the plasma membrane may use distinct motifs for sorting, such as a dileucine motif in ZIP1 (Huang and Kirschke, 2007), if they are similarly internalized upon zinc repletion. Markedly, the L2 is the most divergent segment in the TMD among the hZIPs, supporting a notion that this least conserved loop is a key element in specific regulation for each ZIP protein (Bafaro et al., 2015; Bowers and Srai, 2018).

STAR★METHODS

Detailed methods are provided in the online version of this paper and include the following:

LEAD CONTACT AND MATERIALS AVAILABILITY

Further information and requests for resources and reagents should be directed to the Lead Contact, Dr. Jian Hu (hujian1@msu.edu) and will be fulfilled upon completion of a Materials Transfer Agreement.

EXPERIMENTAL MODEL AND SUBJECT DETAILS

Cell Lines—Human embryonic kidney cells (HEK293 and HEK293T, ATCC, Cat#CRL-1573 and #CRL-3216) were cultured in Dulbecco's modified eagle medium (DMEM, Thermo Fisher Scientific, Invitrogen, Cat#11965092) supplemented with 10% (v/v) fetal bovine serum (Thermo Fisher Scientific, Invitrogen, Cat#10082147) and Antibiotic-Antimycotic solution (Thermo Fisher Scientific, Invitrogen, Cat# 15240062) at 5% CO_2 and 37°C. Freestyle 293-F cells were cultured in FreeStyle 293 Expression Medium (Thermo Fisher Scientific, Invitrogen, Cat# 12338026) at 8% CO_2 and 37°C with 150 rpm shaking.

Genes and Plasmids—The complementary DNAs of human ZIP4 (GenBank code: BC062625) and human CD8a (cDNA clone MGC:34614 IMAGE:5227906) from Mammalian Gene Collection were purchased from GE Healthcare. hZIP4 and CD8 were sub-cloned into a modified pEGFP-N1 vector (Clonetech, Cat# 6085–1) in which the downstream EGFP gene was deleted and an HA tag was inserted before the stop codon. All the mutations were made using PfuTurbo DNA polymerase (Agilent, Cat# 600250) and verified by DNA sequencing. All the plasmids were purified using miniprep (Promega, Cat# A1460) or maxiprep (QIAGEN, Cat# 12163).

METHOD DETAILS

Generate stable populations and transient transfection—To generate the stable populations, HEK293 (ATCC, Cat# CRL-1573, RRID:CVCL_0045) cells were plated on 6-well cell culture plate the day before transfection. 2 μg of DNA and 4 μg of Lipofectamine 2000 reagent (Thermo Fisher Scientific, Invitrogen, Cat# 11668019) were used to transfect cells in each well. 24 hours after transfection, cells were expanded to a 100 mm cell culture dish. 500 μg/ml of Geneticin (Thermo Fisher Scientific, Invitrogen, Cat# 11811031) was added in the growth medium 48 hours after transfection. HEK293T cells for transient expression were transfected with 0.5 μg of DNA and 1μg of lipofectamine in each well of a 24-well plate. Cells were treated 24 hours after transfection. Zinc depletion medium (Chelex-treated medium) was prepared using Chelex 100 (Sigma-Aldrich, Cat# C7901–25G). A suspension of 1.3% (w/v) Chelex 100 resin in DMEM medium supplemented with 10% fetal bovine serum was incubated for overnight at 4°C with constant gentle shaking, followed by sedimentation and filtration through a 0.22 μm filter.

hZIP4-HA internalization assay and western blot—Endocytosis of hZIP4-HA was determined by measuring the internalized anti-HA antibody (Thermo Fisher Scientific,

Cat#26183) added to the cells stably or transiently expressing hZIP4-HA or the variants. We followed the previously established protocols with small modifications (Chun et al., 2019; Kim et al., 2004; Mao et al., 2007; Wang et al., 2004b; Weaver et al., 2007). In brief, cells were seeded on poly-D-lysine (Corning, Cat# 354210) coated 24-wells trays for 16 hours in the basal medium. Unless indicated otherwise, cells were incubated with 20 μM N,N,N',N'-tetrakis(2-pyridylmethyl)ethane-1,2-diamine (TPEN) (Sigma-Aldrich, Cat# **P4413**) for 15 min at 37°C, washed one time with the Chelex-treated medium and then cells were incubated for 30 min at 37°C in the Chelex-treated medium containing 4 μg/ml anti-HA antibodies without or with the indicated amounts of zinc chloride. The time-course experiment indicated that anti-HA internalization is linear up to 30 minutes with or without TPEN treatment (Figure S3), so 30-minute incubation was used in all the internalization assays. Cells were chilled on ice to stop protein trafficking and washed one time with 0.6 mL of Dulbecco's phosphate-buffered saline (DPBS) (Sigma-Aldrich, Cat# D8537–500ML) on ice. The surface-bound antibodies were removed by five washes with 0.6 mL of ice-cold acidic buffer (100 mM glycine, 20 mM magnesium acetate, 50 mM potassium chloride, pH 2.2) and three times washes in DPBS. Cells in each well were harvested and solubilized in 100 μl SDS–PAGE sample loading buffer.

All the samples were heated at 96°C for 6 min. Cell lysate containing the internalized anti-HA antibody were applied to SDS-PAGE. The proteins were transferred to PVDF membranes (Millipore, Cat# PVH00010) for western blot assay by chemiluminescence using horseradish peroxidase-conjugated goat anti-mouse immunoglobulin-G at 1:2,500 (Cell Signaling Technoloy, Cat# 7076S RRID:AB_330924). Total expressions were analyzed using anti-HA antibodies at 1:5,000. As loading control, β-actin levels were detected using an anti-b-actin antibody at 1:2,500 (Cell Signaling Technology, Cat# 4970). Bound primary antibody was detected with HRP-conjugated goat anti-mouse immunoglobulin-G (1:6,000) or goat anti-rabbit immunoglobulin-G at 1:2,500 (Cell Signaling Technology, Cat# 7074S, RRID:AB_2099233) by chemiluminescence (VWR, Cat# RPN2232). The blots were taken using a Bio-Rad ChemiDoc Imaging System.

The zinc sensing capability is calculated using the following equation:

$$\text{Zinc Sensing Capability} = (\text{Ab}_{\text{Zn}} - \text{Ab}_{\text{No}-\text{Zn}})/\text{Ab}_{\text{Zn}}$$

Where Ab_{Zn} refers to the internalized anti-HA antibody in the presence of 10 μM added zinc chloride in the Chelex-treated medium and $\text{Ab}_{\text{No\_Zn}}$ is the internalized anti-HA antibody in the absence of added zinc in the Chelex-treated medium.

hZIP4-HA surface expression detection—hZIP4-HA expressed at the plasma membrane was indicated by the surface bound anti-HA antibodies recognizing the C-terminal HA tag of hZIP4. Cells were seeded on coated 24-wells trays for 16 hours in basal medium. After washing twice with DPBS on ice, cells were fixed for 10 min in 4% formaldehyde at room temperature. Cells were then washed three times in DPBS and incubated with 3 μg/ml anti-HA antibody diluted with 5% BSA in DPBS one hour and a half at room temperature. Cells were washed five times with DPBS to remove unbound

antibodies and then lysed in SDS–PAGE loading buffer. The anti-HA antibody bound to the surface hZIP4-HA in cell lysates were detected in western blot with HRP-conjugated goat anti-mouse immunoglobulin-G (1:2,500) or goat anti-rabbit immunoglobulin-G (1:3,000) by chemiluminescence. As loading control, β-actin levels were detected using an anti-β-actin antibody (1:2,500).

Analysis of internalized anti-HA antibody using immunofluoresence microscopy—HEK293 cells stably expressing hZIP4-HA were grown in 24-well trays for 16 h on sterile glass coverslips. For the basal condition, the cells were incubated in the basal medium with 4 μg/ml anti-HA antibodies at 37°C for 30 min. For the other conditions, the cells were first treated with 20 μM TPEN for 10 min at 37°C, washed one time with the Chelex-treated medium and then incubated for 30 min at 37°C in the Chelex-treated medium containing 4 μg/ml anti-HA antibodies without or with 10 μM $ZnCl_2$. For transferrin internalization assay, the cells were treated in the same way under the same condition, except that 25 μg/ml Alexa 488 conjugated transferrin (Thermo Fisher Scientific,Cat# T13342) was added in the medium instead of anti-HA antibodies. The cells were washed twice with 1 mL of ice-cold DPBS and fixed for 10 min at room temperature using 4% formaldehyde. They were then permeabilized and blocked for 1h with DPBS containing 5% goat serum (Cell Signaling Technology, Cat# 5425S) and 0.1% Triton X-100 and then incubated with Alexa-568 goat anti-mouse antibodies at 1:500 (Thermo Fisher Scientific, Cat# A-11004, RRID:AB_2534072) at 4°C for overnight. After three washes with DPBS, coverslips were mounted on slides with fluoroshield mounting medium with DAPI (Abcam, Cat# ab104139). Samples were viewed with a 63X objective using a Zeiss Axio fluorescence microscope.

FLAG-hZIP4-HA expression and purification—FLAG-hZIP4-HA was transiently expressed in Freestyle 293-F cells. For transfections, 1 μg/ml FLAG-hZIP4-HA plasmid DNA was mixed with 3 μg/ml Polyethylenimine (PEI) (25 kDa linear PEI, Polysciences, Cat# 23966) at room temperature for 30 min. The DNA-PEI mixture was added to cells at a density of 1.5×10^6 cells/ml. The cells were allowed to grow for 3 days before harvest. Cell pellets were lysed in the buffer (50mM Tris, pH 7.5, 300mM NaCl, 5% glycerol, 1% DDM (Anatrace, Cat#69227–93-6) in presence of *FAST*ä protease inhibitor (Sigma-Aldrich, Cat# S8830) and the cell lysate was centrifuged for 30 min at 10,000 rpm. The supernatant was incubated with the anti-FLAG M2 affinity resin (Sigma-Aldrich, Cat# A2220) for 1 hour on at 4°C with gentle shaking. After washing for 6 times with the cold purification buffer (50 mM Tris, pH 7.5, 300 mM NaCl, 5% glycerol, 0.05% DDM), FLAG-hZIP4-HA were eluted with the elution buffer containing 100 μg/ml FLAG peptide (Sigma-Aldrich, Cat# F3290). The protein was further purified using size exclusion chromatography to remove aggregates.

Partial proteolysis and mass spectrometry—To optimize the reaction condition, chymotrypsin dissolved in the purification buffer with various concentrations was added to the purified FLAG-hZIP4-HA in 50 mM Tris, pH 7.5, 300 mM NaCl, 5% glycerol, 0.05% DDM. After incubation at room temperature for 20 min, the reaction was terminated by adding SDS-PAGE sample loading buffer containing 1 mM PMSF (Thermo Fisher Scientific, Cat#36978). The proteolytic products were then detected in western blot using

anti-FLAG antibody (Agilent, Cat# 200474) for the N-terminal fragment(s) or anti-HA antibody for the C-terminal fragment(s). Partial proteolysis fragments were also detected by LC/MS/MS using Mascot (Matrix Science, London, UK; version 2.6.0) and X! Tandem (The GPM; version X! Tandem Alanine 2017.2.1.4). To test the effects of zinc ions on partial proteolysis, the reaction was performed in the presence of indicated concentrations of $ZnSO_4$ at the optimized protein:chymotrypsin ratio and the proteolytic products were detected in western blot.

QUANTIFICATION AND STATISTICAL ANALYSIS

All the blots were analyzed by ImageJ for quantification of western blot signals. Statistical tests were performed in Graphpad Prism 5. At least three independent experiments were performed and data were presented as mean ± standard deviation. We assumed a normal distribution of the samples and multiple comparisons were assessed usingStudent's t test. A $p < 0.05$ was considered statistically significant.

Supplementary Material

Refer to Web version on PubMed Central for supplementary material.

ACKNOWLEDGMENTS

DATA AND CODE AVAILABILITY

Original western blot data are deposited on Mendeley (https://data.mendeley.com/datasets/2fck9mdb2s/1).

REFERENCES

Andrews GK (2008). Regulation and function of Zip4, the acrodermatitis enteropathica gene. Biochem. Soc. Trans. 36, 1242–1246. [PubMed: 19021533]

Antala S, and Dempski RE (2012). The human ZIP4 transporter has two distinct binding affinities and mediates transport of multiple transition metals. Biochemistry 51, 963–973. [PubMed: 22242765]

Antala S, Ovchinnikov S, Kamisetty H, Baker D, and Dempski RE (2015). Computation and Functional Studies Provide a Model for the Structure of the Zinc Transporter hZIP4. J. Biol. Chem. 290, 17796–17805. [PubMed: 25971965]

Bafaro EM, Antala S, Nguyen TV, Dzul SP, Doyon B, Stemmler TL, and Dempski RE (2015). The large intracellular loop of hZIP4 is an intrinsically disordered zinc binding domain. Metallomics 7, 1319–1330. [PubMed: 25882556]

Bafaro E, Liu Y, Xu Y, and Dempski RE (2017). The emerging role of zinc transporters in cellular homeostasis and cancer. Signal Transduct. Target. Ther. 2, 17029. [PubMed: 29218234]

Bafaro EM, Maciejewski MW, Hoch JC, and Dempski RE (2019). Concomitant disorder and high-affinity zinc binding in the human zinc- and iron-regulated transport protein 4 intracellular loop. Protein Sci. 28, 868–880. [PubMed: 30793391]

Bowers K, and Srai SKS (2018). The trafficking of metal ion transporters of the Zrt- and Irt-like protein family. Traffic 19, 813–822. [PubMed: 29952128]

Cain NE, and Kaiser CA (2011). Transport activity-dependent intracellular sorting of the yeast general amino acid permease. Mol. Biol. Cell 22, 1919–1929. [PubMed: 21471002]

Chowanadisai W, Graham DM, Keen CL, Rucker RB, and Messerli MA (2013). Neurulation and neurite extension require the zinc transporter ZIP12 (slc39a12). Proc. Natl. Acad. Sci. USA 110, 9903–9908. [PubMed: 23716681]

Chun H, Korolnek T, Lee CJ, Coyne HJ 3rd, Winge DR, Kim BE, and Petris MJ (2019). An extracellular histidine-containing motif in the zinc transporter ZIP4 plays a role in zinc sensing and zinc-induced endocytosis in mammalian cells. J. Biol. Chem. 294, 2815–2826. [PubMed: 30593504]

Clifford RJ, Maryon EB, and Kaplan JH (2016). Dynamic internalization and recycling of a metal ion transporter: Cu homeostasis and CTR1, the human Cu^+ uptake system. J. Cell Sci. 129, 1711–1721. [PubMed: 26945057]

Connolly EL, Fett JP, and Guerinot ML (2002). Expression of the IRT1 metal transporter is controlled by metals at the levels of transcript and protein accumulation. Plant Cell 14, 1347–1357. [PubMed: 12084831]

Dubeaux G, Neveu J, Zelazny E, and Vert G (2018). Metal Sensing by the IRT1 Transporter-Receptor Orchestrates Its Own Degradation and Plant Metal Nutrition. Mol. Cell. 69, 953–964.e5. [PubMed: 29547723]

Dufner-Beattie J, Wang F, Kuo YM, Gitschier J, Eide D, and Andrews GK (2003). The acrodermatitis enteropathica gene ZIP4 encodes a tissue-specific, zinc-regulated zinc transporter in mice. J. Biol. Chem. 278, 33474–33481. [PubMed: 12801924]

Dufner-Beattie J, Weaver BP, Geiser J, Bilgen M, Larson M, Xu W, and Andrews GK (2007). The mouse acrodermatitis enteropathica gene Slc39a4 (Zip4) is essential for early development and heterozygosity causes hypersensitivity to zinc deficiency. Hum. Mol. Genet. 16, 1391–1399. [PubMed: 17483098]

Eguez L, Chung YS, Kuchibhatla A, Paidhungat M, and Garrett S (2004). Yeast Mn2+ transporter, Smf1p, is regulated by ubiquitin-dependent vacuolar protein sorting. Genetics 167, 107–117. [PubMed: 15166140]

Eide D, Broderius M, Fett J, and Guerinot ML (1996). A novel iron-regulated metal transporter from plants identified by functional expression in yeast. Proc. Natl. Acad. Sci. USA 93, 5624–5628. [PubMed: 8643627]

Erpapazoglou Z, Froissard M, Nondier I, Lesuisse E, Haguenauer-Tsapis R, and Belgareh-Touzé N (2008). Substrate- and ubiquitin-dependent trafficking of the yeast siderophore transporter Sit1. Traffic 9, 1372–1391. [PubMed: 18489705]

Felice MR, De Domenico I, Li L, Ward DM, Bartok B, Musci G, and Kaplan J (2005). Post-transcriptional regulation of the yeast high affinity iron transport system. J. Biol. Chem. 280, 22181–22190. [PubMed: 15817488]

Fujita S, Sato D, Kasai H, Ohashi M, Tsukue S, Takekoshi Y, Gomi K, and Shintani T (2018). The C-terminal region of the yeast monocarboxylate transporter Jen1 acts as a glucose signal-responding degron recognized by the α-arrestin Rod1. J. Biol. Chem. 293, 10926–10936. [PubMed: 29789424]

Gaither LA, and Eide DJ (2001). The human ZIP1 transporter mediates zinc uptake in human K562 erythroleukemia cells. J. Biol. Chem. 276, 22258–22264. [PubMed: 11301334]

Galan JM, Moreau V, Andre B, Volland C, and Haguenauer-Tsapis R (1996). Ubiquitination mediated by the Npi1p/Rsp5p ubiquitin-protein ligase is required for endocytosis of the yeast uracil permease. J. Biol. Chem. 271, 10946–10952. [PubMed: 8631913]

Geiser J, Venken KJ, De Lisle RC, and Andrews GK (2012). A mouse model of acrodermatitis enteropathica: loss of intestine zinc transporter ZIP4 (Slc39a4) disrupts the stem cell niche and intestine integrity. PLoS Genet. 8, e1002766. [PubMed: 22737083]

Ghaddar K, Merhi A, Saliba E, Krammer EM, Prévost M, and André B (2014). Substrate-induced ubiquitylation and endocytosis of yeast amino acid permeases. Mol. Cell. Biol. 34, 4447–4463. [PubMed: 25266656]

Gitan RS, and Eide DJ (2000). Zinc-regulated ubiquitin conjugation signals endocytosis of the yeast ZRT1 zinc transporter. Biochem. J. 346, 329–336. [PubMed: 10677350]

Goumakos W, Laussac JP, and Sarkar B (1991). Binding of cadmium(II) and zinc(II) to human and dog serum albumins. An equilibrium dialysis and 113Cd-NMR study. Biochem. Cell Biol. 69, 809–820. [PubMed: 1818586]

Gournas C, Saliba E, Krammer EM, Barthelemy C, Prévost M, and André B (2017). Transition of yeast Can1 transporter to the inward-facing state unveils an α-arrestin target sequence promoting its ubiquitylation and endocytosis. Mol. Biol. Cell 28, 2819–2832. [PubMed: 28814503]

Graschopf A, Stadler JA, Hoellerer MK, Eder S, Sieghardt M, Kohlwein SD, and Schweyen RJ (2001). The yeast plasma membrane protein Alr1 controls Mg2+ homeostasis and is subject to Mg2+-dependent control of its synthesis and degradation. J. Biol. Chem. 276, 16216–16222. [PubMed: 11279208]

Grotz N, Fox T, Connolly E, Park W, Guerinot ML, and Eide D (1998). Identification of a family of zinc transporter genes from Arabidopsis that respond to zinc deficiency. Proc. Natl. Acad. Sci. USA 95, 7220–7224. [PubMed: 9618566]

Guiney EL, Klecker T, and Emr SD (2016). Identification of the endocytic sorting signal recognized by the Art1-Rsp5 ubiquitin ligase complex. Mol. Biol. Cell 27, 4043–4054. [PubMed: 27798240]

Guo Y, Smith K, Lee J, Thiele DJ, and Petris MJ (2004). Identification of methionine-rich clusters that regulate copper-stimulated endocytosis of the human Ctr1 copper transporter. J. Biol. Chem. 279, 17428–17433. [PubMed: 14976198]

Hara T, Takeda TA, Takagishi T, Fukue K, Kambe T, and Fukada T (2017). Physiological roles of zinc transporters: molecular and genetic importance in zinc homeostasis. J. Physiol. Sci. 67, 283–301. [PubMed: 28130681]

Harasaki K, Lubben NB, Harbour M, Taylor MJ, and Robinson MS (2005). Sorting of major cargo glycoproteins into clathrin-coated vesicles. Traffic 6, 1014–1026. [PubMed: 16190982]

Hashimoto A, Ohkura K, Takahashi M, Kizu K, Narita H, Enomoto S, Miyamae Y, Masuda S, Nagao M, Irie K, et al. (2015). Soybean extracts increase cell surface ZIP4 abundance and cellular zinc levels: a potential novel strategy to enhance zinc absorption by ZIP4 targeting. Biochem. J. 472, 183–193. [PubMed: 26385990]

Hashimoto A, Nakagawa M, Tsujimura N, Miyazaki S, Kizu K, Goto T, Komatsu Y, Matsunaga A, Shirakawa H, Narita H, et al. (2016). Properties of Zip4 accumulation during zinc deficiency and its usefulness to evaluate zinc status: a study of the effects of zinc deficiency during lactation. Am. J. Physiol. Regul. Integr. Comp. Physiol. 310, R459–R468. [PubMed: 26702153]

Huang L, and Kirschke CP (2007). A di-leucine sorting signal in ZIP1 (SLC39A1) mediates endocytosis of the protein. FEBS J. 274, 3986–3997. [PubMed: 17635580]

Jeong J, and Eide DJ (2013). The SLC39 family of zinc transporters. Mol. Aspects Med. 34, 612–619. [PubMed: 23506894]

Kambe T, and Andrews GK (2009). Novel proteolytic processing of the ectodomain of the zinc transporter ZIP4 (SLC39A4) during zinc deficiency is inhibited by acrodermatitis enteropathica mutations. Mol. Cell. Biol. 29, 129–139. [PubMed: 18936158]

Kambe T, Yamaguchi-Iwai Y, Sasaki R, and Nagao M (2004). Overview of mammalian zinc transporters. Cell. Mol. Life Sci. 61, 49–68. [PubMed: 14704853]

Kambe T, Hashimoto A, and Fujimoto S (2014). Current understanding of ZIP and ZnT zinc transporters in human health and diseases. Cell. Mol. Life Sci. 71, 3281–3295. [PubMed: 24710731]

Kambe T, Tsuji T, Hashimoto A, and Itsumura N (2015). The Physiological, Biochemical, and Molecular Roles of Zinc Transporters in Zinc Homeostasis and Metabolism. Physiol. Rev. 95, 749–784. [PubMed: 26084690]

Keener JM, and Babst M (2013). Quality control and substrate-dependent downregulation of the nutrient transporter Fur4. Traffic 14, 412–427. [PubMed: 23305501]

Kim BE, Wang F, Dufner-Beattie J, Andrews GK, Eide DJ, and Petris MJ (2004). Zn2+-stimulated endocytosis of the mZIP4 zinc transporter regulates its location at the plasma membrane. J. Biol. Chem. 279, 4523–4530. [PubMed: 14612438]

Kozik P, Francis RW, Seaman MN, and Robinson MS (2010). A screen for endocytic motifs. Traffic 11, 843–855. [PubMed: 20214754]

Küry S, Dréno B, Bézieau S, Giraudet S, Kharfi M, Kamoun R, and Moisan JP (2002). Identification of SLC39A4, a gene involved in acrodermatitis enteropathica. Nat. Genet. 31, 239–240. [PubMed: 12068297]

Lichten LA, and Cousins RJ (2009). Mammalian zinc transporters: nutritional and physiologic regulation. Annu. Rev. Nutr. 29, 153–176. [PubMed: 19400752]

Liu J, Sitaram A, and Burd CG (2007). Regulation of copper-dependent endocytosis and vacuolar degradation of the yeast copper transporter, Ctr1p, by the Rsp5 ubiquitin ligase. Traffic 8, 1375–1384. [PubMed: 17645432]

Liu Z, Li H, Soleimani M, Girijashanker K, Reed JM, He L, Dalton TP, and Nebert DW (2008). Cd2+ versus Zn2+ uptake by the ZIP8 HCO3–dependent symporter: kinetics, electrogenicity and trafficking. Biochem. Biophys. Res. Commun. 365, 814–820. [PubMed: 18037372]

Liuzzi JP, and Cousins RJ (2004). Mammalian zinc transporters. Annu. Rev. Nutr. 24, 151–172. [PubMed: 15189117]

Liuzzi JP, Guo L, Chang SM, and Cousins RJ (2009). Krüppel-like factor 4 regulates adaptive expression of the zinc transporter Zip4 in mouse small intestine. Am. J. Physiol. Gastrointest. Liver Physiol. 296, G517–G523. [PubMed: 19147802]

Lu J, Stewart AJ, Sadler PJ, Pinheiro TJ, and Blindauer CA (2008). Albumin as a zinc carrier: properties of its high-affinity zinc-binding site. Biochem. Soc. Trans. 36, 1317–1321. [PubMed: 19021548]

Mao X, Kim BE, Wang F, Eide DJ, and Petris MJ (2007). A histidine-rich cluster mediates the ubiquitination and degradation of the human zinc transporter, hZIP4, and protects against zinc cytotoxicity. J. Biol. Chem. 282, 6992–7000. [PubMed: 17202136]

Miller SE, Sahlender DA, Graham SC, Höning S, Robinson MS, Peden AA, and Owen DJ (2011). The molecular basis for the endocytosis of small R-SNAREs by the clathrin adaptor CALM. Cell 147, 1118–1131. [PubMed: 22118466]

Milon B, Dhermy D, Pountney D, Bourgeois M, and Beaumont C (2001). Differential subcellular localization of hZip1 in adherent and non-adherent cells. FEBS Lett. 507, 241–246. [PubMed: 11696349]

Molloy SA, and Kaplan JH (2009). Copper-dependent recycling of hCTR1, the human high affinity copper transporter. J. Biol. Chem. 284, 29704–29713. [PubMed: 19740744]

Nilsson T, Jackson M, and Peterson PA (1989). Short cytoplasmic sequences serve as retention signals for transmembrane proteins in the endoplasmic reticulum. Cell 58, 707–718. [PubMed: 2527615]

Pocanschi CL, Ehsani S, Mehrabian M, Wille H, Reginold W, Trimble WS, Wang H, Yee A, Arrowsmith CH, Bozóky Z, et al. (2013). The ZIP5 ectodomain co-localizes with PrP and may acquire a PrP-like fold that assembles into a dimer. PLoS ONE 8, e72446. [PubMed: 24039764]

Pryor PR, Jackson L, Gray SR, Edeling MA, Thompson A, Sanderson CM, Evans PR, Owen DJ, and Luzio JP (2008). Molecular basis for the sorting of the SNARE VAMP7 into endocytic clathrin-coated vesicles by the ArfGAP Hrb. Cell 134, 817–827. [PubMed: 18775314]

Richardson CER, Cunden LS, Butty VL, Nolan EM, Lippard SJ, and Shoulders MD (2018). A Method for Selective Depletion of Zn(II) Ions from Complex Biological Media and Evaluation of Cellular Consequences of Zn(II) Deficiency. J. Am. Chem. Soc. 140, 2413–2416. [PubMed: 29334734]

Rogers EE, Eide DJ, and Guerinot ML (2000). Altered selectivity in an Arabidopsis metal transporter. Proc. Natl. Acad. Sci. USA 97, 12356–12360. [PubMed: 11035780]

Seaman MN (2007). Identification of a novel conserved sorting motif required for retromer-mediated endosome-to-TGN retrieval. J. Cell Sci. 120, 2378–2389. [PubMed: 17606993]

Soetens O, De Craene JO, and Andre B (2001). Ubiquitin is required for sorting to the vacuole of the yeast general amino acid permease, Gap1. J. Biol. Chem. 276, 43949–43957. [PubMed: 11500494]

Takagishi T, Hara T, and Fukada T (2017). Recent Advances in the Role of SLC39A/ZIP Zinc Transporters In Vivo. Int. J. Mol. Sci. 18, e2708. [PubMed: 29236063]

Talaia G, Gournas C, Saliba E, Barata-Antunes C, Casal M, André B, Diallinas G, and Paiva S (2017). The α-Arrestin Bul1p Mediates Lactate Transporter Endocytosis in Response to Alkalinization and Distinct Physiological Signals. J. Mol. Biol. 429, 3678–3695. [PubMed: 28965784]

Traub LM, and Bonifacino JS (2013). Cargo recognition in clathrin-mediated endocytosis. Cold Spring Harb. Perspect. Biol. 5, a016790. [PubMed: 24186068]

Vercauteren D, Vandenbroucke RE, Jones AT, Rejman J, Demeester J, De Smedt SC, Sanders NN, and Braeckmans K (2010). The use of inhibitors to study endocytic pathways of gene carriers: optimization and pitfalls. Mol. Ther. 18, 561–569. [PubMed: 20010917]

Wang K, Zhou B, Kuo YM, Zemansky J, and Gitschier J (2002). A novel member of a zinc transporter family is defective in acrodermatitis enteropathica. Am. J. Hum. Genet. 71, 66–73. [PubMed: 12032886]

Wang F, Dufner-Beattie J, Kim BE, Petris MJ, Andrews G, and Eide DJ (2004a). Zinc-stimulated endocytosis controls activity of the mouse ZIP1 and ZIP3 zinc uptake transporters. J. Biol. Chem. 279, 24631–24639. [PubMed: 15054103]

Wang F, Kim BE, Dufner-Beattie J, Petris MJ, Andrews G, and Eide DJ (2004b). Acrodermatitis enteropathica mutations affect transport activity, localization and zinc-responsive trafficking of the mouse ZIP4 zinc transporter. Hum. Mol. Genet. 13, 563–571. [PubMed: 14709598]

Weaver BP, and Andrews GK (2012). Regulation of zinc-responsive Slc39a5 (Zip5) translation is mediated by conserved elements in the 3′-untranslated region. Biometals 25, 319–335. [PubMed: 22113231]

Weaver BP, Dufner-Beattie J, Kambe T, and Andrews GK (2007). Novel zinc-responsive post-transcriptional mechanisms reciprocally regulate expression of the mouse Slc39a4 and Slc39a5 zinc transporters (Zip4 and Zip5). Biol. Chem. 388, 1301–1312. [PubMed: 18020946]

Yu A, Xing Y, Harrison SC, and Kirchhausen T (2010). Structural analysis of the interaction between Dishevelled2 and clathrin AP-2 adaptor, a critical step in noncanonical Wnt signaling. Structure 18, 1311–1320. [PubMed: 20947020]

Zhang T, Sui D, and Hu J (2016). Structural insights of ZIP4 extracellular domain critical for optimal zinc transport. Nat. Commun. 7, 11979. [PubMed: 27321477]

Zhang T, Liu J, Fellner M, Zhang C, Sui D, and Hu J (2017). Crystal structures of a ZIP zinc transporter reveal a binuclear metal center in the transport pathway. Sci. Adv. 3, e1700344. [PubMed: 28875161]

Zhang T, Kuliyev E, Sui D, and Hu J (2019). The histidine-rich loop in the extracellular domain of ZIP4 binds zinc and plays a role in zinc transport. Biochem. J. 476, 1791–1803. [PubMed: 31164399]

Zhao N, Zhang AS, Worthen C, Knutson MD, and Enns CA (2014). An iron-regulated and glycosylation-dependent proteasomal degradation pathway for the plasma membrane metal transporter ZIP14. Proc. Natl. Acad. Sci. USA 111, 9175–9180. [PubMed: 24927598]

Highlights

- Depletion of extracellular/intracellular zinc pools drastically reduces ZIP4 endocytosis

- ZIP4 utilizes the transport site to sense zinc in the zinc-dependent endocytosis

- An LQL motif in the L2 cytosolic loop is essential for ZIP4 endocytosis

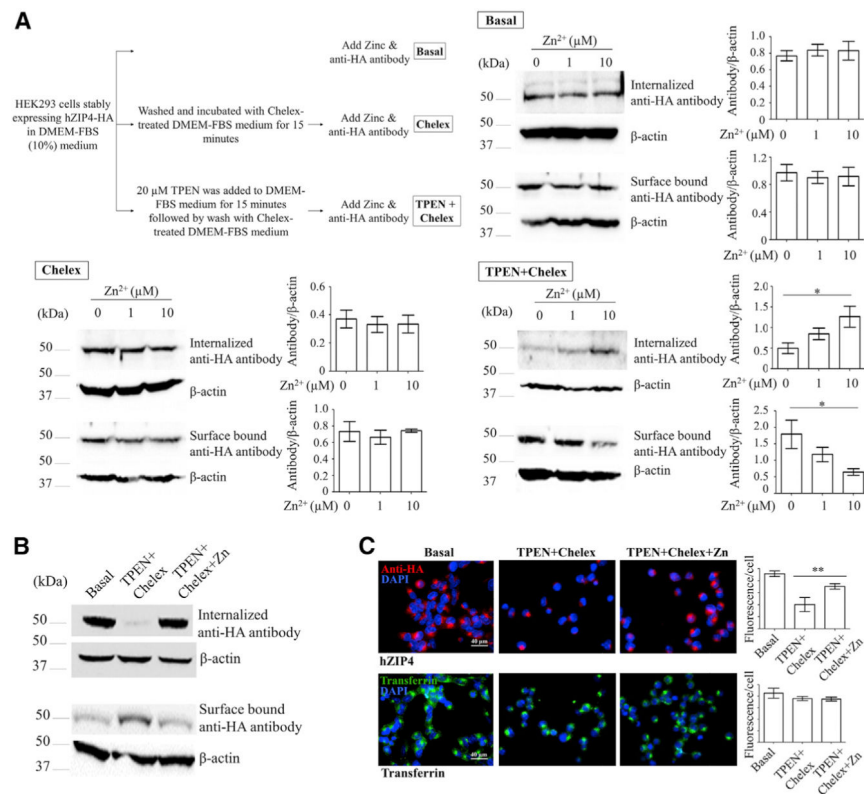- The transport site and the L2 loop are structurally coupled

Figure 1. Characterization of Zinc-Dependent Constitutive Endocytosis of hZIP4 Stably Expressed in HEK293 Cells

(A) The effects of zinc chloride on hZIP4 endocytosis. As shown in the flowchart (upper left panel), the cells stably expressing hZIP4-HA were treated differently (basal, Chelex, and TPEN+Chelex) before zinc and anti-HA antibody were added to initiate internalization assay. Zinc had no effect on hZIP4 endocytosis only when both extracellular and intracellular zinc pools were depleted by TPEN. hZIP4-HA cell surface expression level was detected by surface-bound anti-HA antibody, and the endocytosis level was measured by internalized anti-HA antibody. Statistical analysis of 3–6 independent experiments under each condition is shown in the column chart, and the error bar indicates ± 1 SD. *p < 0.05.

(B) Comparison of hZIP4-HA cell surface expression and endocytosis under the basal, zinc-depletion (TPEN+Chelex), and zinc-repletion (TPEN+Chelex+Zn) conditions.

(C) Immuno-fluorescence assay of hZIP4 endocytosis (indicated by internalized anti-HA antibody detected with Alexa 568-labeled secondary antibody, red) and Alexa 488-conjugated transferrin (green) endocytosis. Nucleus is indicated by DAPI (blue). Statistical analysis of 200 cells in each condition is shown in the column chart, and the error bar indicates ± 1 SD. **p < 0.01.
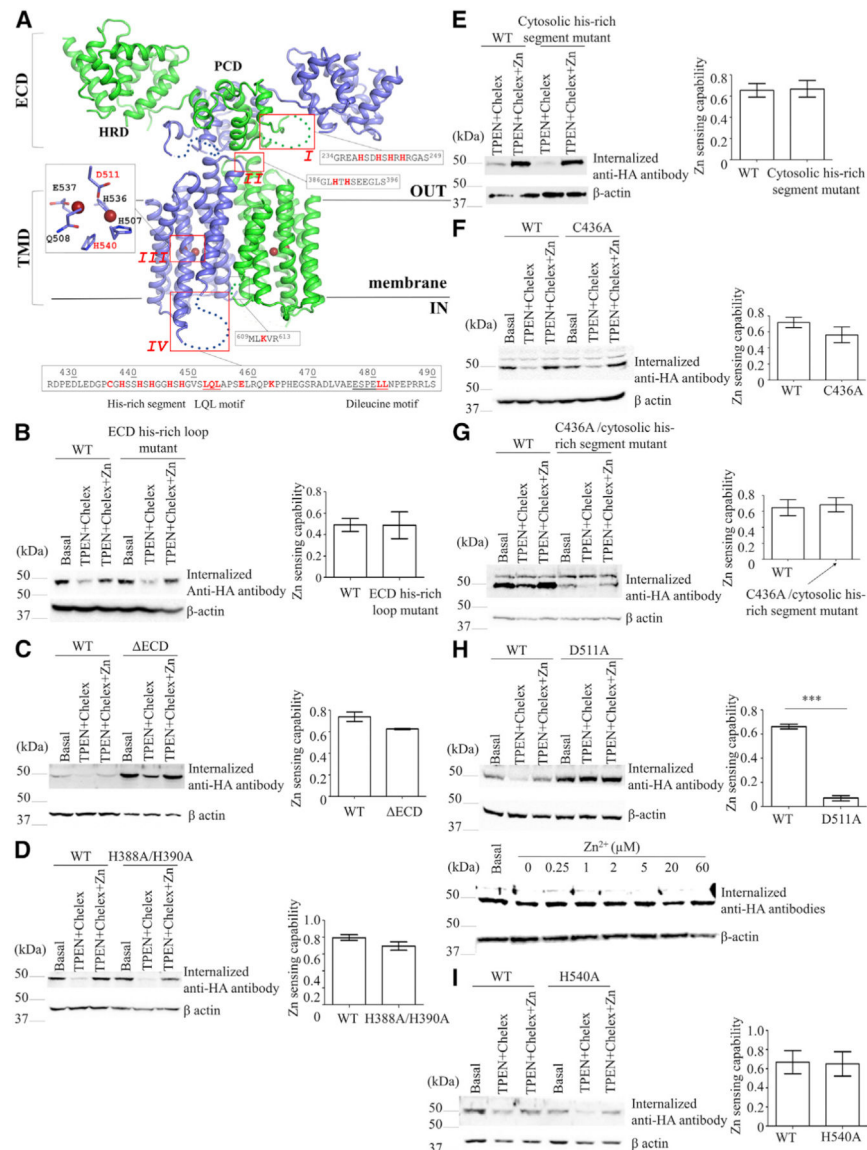
Figure 2. Zinc-Sensing Function of hZIP4 in Zinc-Dependent Endocytosis

(A) Structure model of hZIP4. The protein is shown in cartoon mode, and the disordered segments are indicated by the dotted lines. Four regions containing the potential high-affinity zinc binding sites are labeled. Region I is a histidine-rich segment in the ECD; region II is an HxH motif in the loop connecting TM2 and TM3; region III is the transport site in the TMD; and region IV covers the second cytosolic loop between TM3 and TM4 (L2), which contains the intracellular histidine-rich segment, the LQL motif, a conserved lysine residue (K463) proposed to be ubiquitinated in zinc-induced degradation (Mao et al., 2007), and a putative dileucine sorting motif. The corresponding amino acid sequences of regions I, II, and IV and the structural model of the zinc-bound transport site (region III) are shown in the black frames. The other cytosolic lysine residue (K611) in a short loop connecting TM7 and TM8 is also highlighted. The residues in red were mutated in this work.

(B–I) Internalization assay of the hZIP4 mutants. Except for those under the basal condition, the cells were treated with 20 μM TPEN for 15 min, washed with the Chelex-treated medium, and then incubated with anti-HA antibody in the Chelex-treated medium with and without 10 μM zinc chloride for 30 min. For each mutant, zinc-sensing capability was calculated based on 3–4 independent experiments. The error bars indicate ± 1 SD. ***p < 0.001.

(B) The ECD his-rich loop mutant (H238S/H241S/H243S/H245S).

(C) The ECD mutant.

(D) The H388A/H340A mutant.

(E) The intracellular histidine-rich segment mutant (H438G/H441G/H443G/H446G/ H448G).

(F) The C436A mutant.

(G) The C436A/H438G/H441G/H443G/H446G/H448G mutant.

(H) The D511A mutant.

(I) The H540A mutant. For D511A, the internalization assay was conducted at the indicated zinc concentrations.

The variants in (D)–(G) were transiently expressed in HEK293T cells, and the other variants were stably expressed in HEK293 cells.
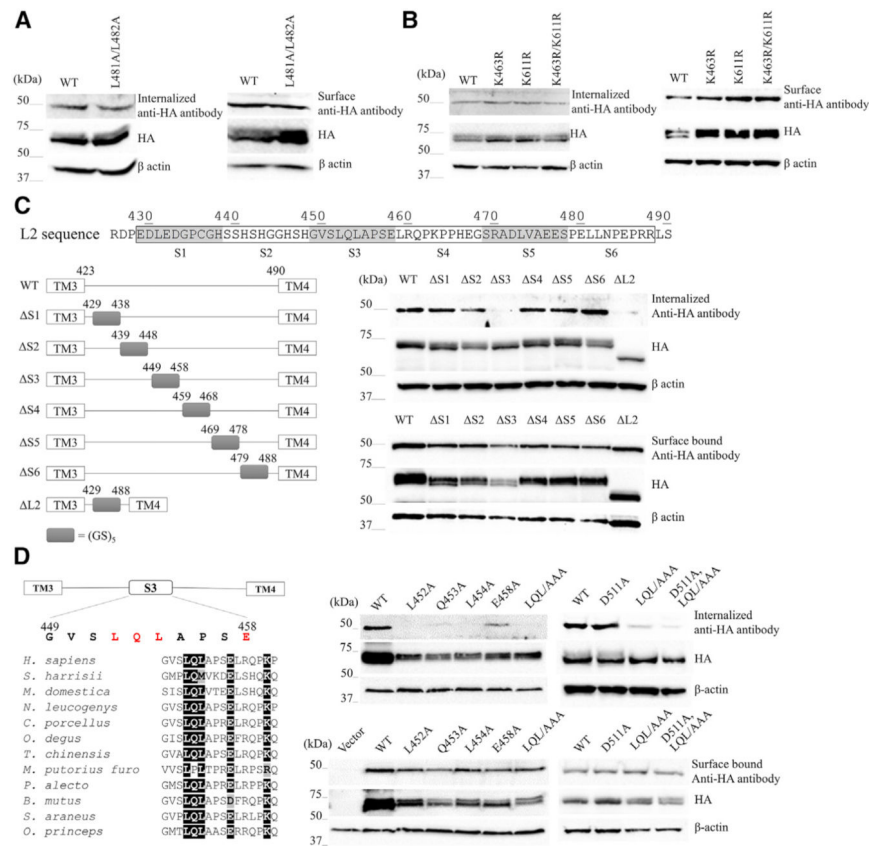
Figure 3. Identification of the LQL Motif Required for Zinc-Dependent hZIP4 Endocytosis

(A and B) Endocytosis, total expression, and surface expression of the dileucine motif mutant (L481A/L482A) (A) and the K463R, K611R, and K463R/K611R mutants (B).

(C) Endocytosis of the L2 mutants. Left: the L2 was divided into six 10-residue segments (S1–S6), and each segment was replaced by a 10-residue (GS)₅ linker to generate six mutants (S1–6), and the whole L2 was replaced by the (GS)₅ linker in the L2 mutant. Right: endocytosis, total expression, and surface expression of the mutants.

(D) Endocytosis of the LQL motif mutants. Left: sequence alignment of the third segment (S3) with highlighted conserved residues. K463 (in S4) is eight residues downstream of the LQL motif. Right: endocytosis, total expression, and surface expression of the LQL motif mutants (L452A, Q453A, L454A, E458A, and the LQL/AAA triple mutant), as well as the D511A/LQL/AAA quadruple mutant.

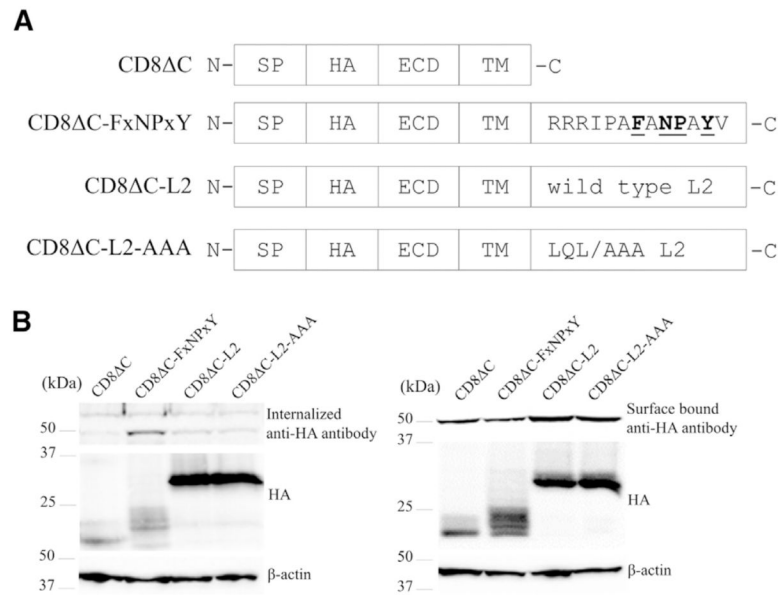The mutants in (A)–(D) were transiently expressed in HEK293T cells.

Figure 4. Examination of the LQL Motif as a Linear Sorting Motif
(A) CD8 chimera constructs. The wild-type L2 is composed of the residues 423–488 of hZIP4, and the LQL motif is replaced by a AAA sequence in the L2 mutant. ECD, extracellular domain of CD8; HA, HA tag; SP, signal peptide of CD8; TM, transmembrane helix plus four cytosolic residues (NHRN) at the C terminus of CD8.
(B) Endocytosis, total expression, and surface expression detection of the CD8 chimeras transiently expressed in HEK293T cells.
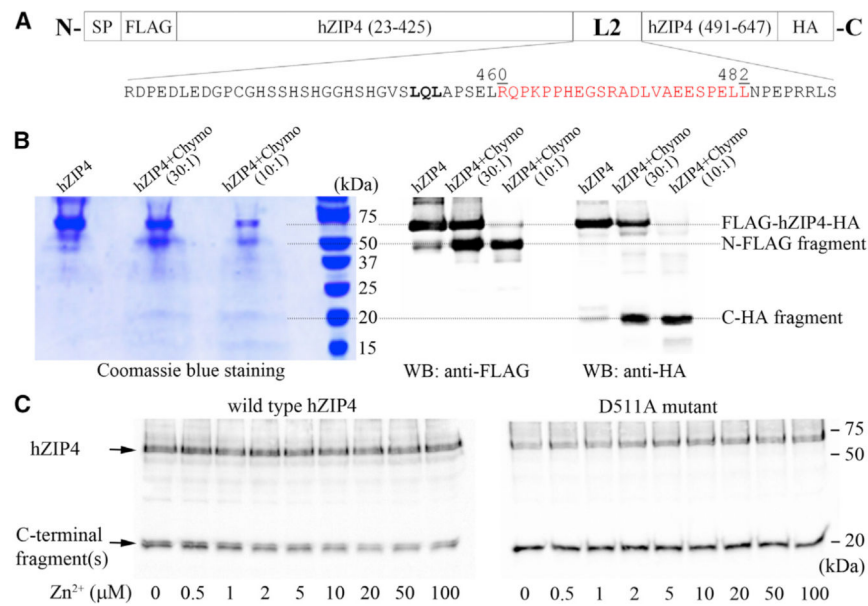
Figure 5. Partial Proteolysis of hZIP4

(A) The FLAG-hZIP4-HA construct. The fragment in red is the peptide identified in mass spectrometry (Figure S5). The LQL motif is in bold. SP, signal peptide of hZIP4 (residues 1–22).

(B) Partial proteolysis of purified hZIP4 by chymotrypsin under optimized condition. Proteolysis products were detected by Coomassie blue staining and western blots using antibodies against FLAG tag or HA tag.

(C) Effects of zinc ions on proteolysis of the wild-type hZIP4 (left) and the D511A mutant (right) detected by western blot against the HA tag. The quantitative analysis of zinc protection for the wild-type protein is shown in Figure S6.
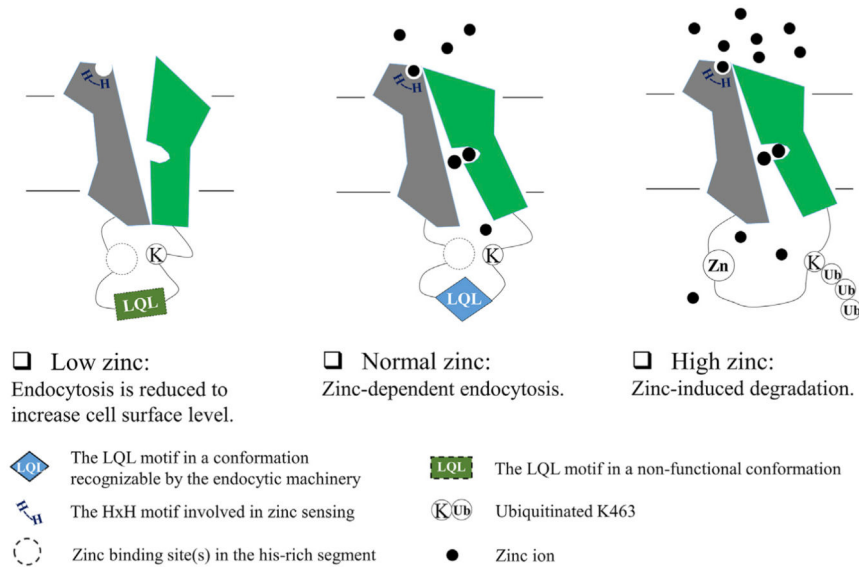
Figure 6. Proposed Working Mechanism of hZIP4 Post-translational Regulation
Under the normal condition with adequate but non-excessive zinc, hZIP4 undergoes a zinc-dependent constitutive endocytosis in a ubiquitin-independent manner (middle). Zinc binding to the transport site, and probably the HxH motif concomitantly, induces a global conformational change, inducing the LQL motif to fold into a conformation so that hZIP4 is recognizable by the endocytic machinery. Upon zinc depletion, the LQL motif may adopt a non-functional conformation due to the lack of zinc binding at the transport site (left). At toxic zinc concentration, intracellular zinc binding to the histidine-rich segment structurally remodels K463, initiating a ubiquitination-dependent zinc-induced degradation (right).

KEY RESOURCES TABLE

REAGENT or RESOURCE	SOURCE	IDENTIFIER
Antibodies		
HA Epitope Tag Antibody (2–2.2.14)	Thermo Fisher Scientific	Cat# 26183; RRID: AB_10978021
beta-actin (13E5) rabbit mAB	Cell Signaling Technology	Cat# 4970S; RRID: AB_2223172
Rat monoclonal antibody to DYKDDDDK eptiope tag	Agilent	Cat# 200474; RRID: AB_10597743
Anti-mouse IgG, HRP-linked Antibody	Cell Signaling Technology	Cat# 7076S
		RRID: AB_330924
Anti-rabbit IgG, HRP-linked Antibody	Cell Signaling Technology	Cat# 7074S
		RRID: AB_2099233
Anti-rat IgG, HRP-linked Antibody	Cell Signaling Technology	Cat# 7077S
		RRID: AB_10694715
Goat anti-Mouse IgG (H+L) Cross-Adsorbed Secondary Antibody, Alexa Fluor 568	Thermo Fisher Scientific	Cat# A-11004, RRID: AB_2534072
Chemicals, Peptides, and Recombinant Proteins		
Dulbecco's Modified Eagle Medium (DMEM)	Thermo Fisher Scientific,Invitrogen	Cat# 11965092
Antibiotic-Antimycotic (100X)	Thermo Fisher Scientific,Invitrogen	Cat# 15240062
FreeStyle 293 Expression Medium	Thermo Fisher Scientific,Invitrogen	Cat# 12338026
Geneticin Selective Antibiotic (G418 Sulfate), Powder	Thermo Fisher Scientific,Invitrogen	Cat# 11811031
Corning BioCoat Poly-D-Lysine	Corning	Cat# 354210
Chelex® 100 sodium form	Sigma-Aldrich	Cat# C7901-25G
N,N,N′,N′-Tetrakis(2-pyridylmethyl) ethylenediamine (TPEN)	Sigma-Aldrich	Cat# P4413
Dulbecco's Phosphate Buffered Saline	Sigma-Aldrich	Cat# D8537-500ML
Immobilon-P PVDF Membrane	Millipore	Cat# PVH00010
Transferrin From Human Serum, Alexa Fluor 488 Conjugate	Thermo Fisher Scientific	Cat# T13342
Normal Goat Serum	Cell Signaling Technology	Cat# 5425S
Mounting Medium With DAPI - Aqueous, Fluoroshield	Abcam	Cat# ab104139
Polyethylenimine, Linear, MW 25000, Transfection Grade (PEI 25K)	Polysciences	Cat# 23966
ANTI-FLAG® M2 Affinity Gel	Sigma-Aldrich	Cat# A2220
Sigma *FAST*ä Protease Inhibitor Cocktail Tablet, EDTA Free	Sigma-Aldrich	Cat# S8830
FLAG® Peptide	Sigma-Aldrich	Cat# F3290-4MG
n-Dodecyl-β-D-Maltopyranoside, Anagrade (DDM)	Anatrace	Cat# 69227-93-6
phenylmethylsulfonyl fluoride (PMSF)	Thermo Fisher Scientific	*Cat# 36978*
Critical Commercial Assays		
PfuTurbo DNA Polymerase	Agilent	Cat# 600250
Wizard® *Plus* SV Minipreps DNA Purification	Promega	Cat# A1460
QIAGEN Plasmid Maxi Kit	QIAGEN	Cat# 12163
Lipofectamine 2000 Transfection Reagent	Thermo Fisher Scientific,Invitrogen	Cat# 11668019
ECL Prime Western Blotting Detection Reagent	VWR	Cat# RPN2232

REAGENT or RESOURCE	SOURCE	IDENTIFIER
Deposited Data		
Original western blots	This paper	Mendeley (http://data.mendeley.com/drafts)
Experimental Models: Cell Lines		
HEK293	ATCC	Cat# CRL-1573, RRID:CVCL_0045
HEK293T	ATCC	Cat# CRL-3216, RRID:CVCL_0063
Freestyle 293-F cells	Thermo Fisher Scientific	SKU# R790-07
Recombinant DNA		
pEGFP-N1	Clonetech	Cat# 6085-1
Software and Algorithms		
ImageJ	NIH	RRID: SCR_003070
GraphPad Prism 5	GraphPad Prism	RRID: SCR_002798